Diamond & Related Materials 61 (2016) 7–13

Contents lists available at ScienceDirect

Diamond & Related Materials

journal homepage: www.elsevier.com/locate/diamond

Solvent–surface interactions between nanodiamond and ethanol studied with *in situ* infrared spectroscopy

Georgiana A. Inel [a], Eleonora-Mihaela Ungureau [a], Thomas S. Varley [b], Meetal Hirani [b], Katherine B. Holt [b,*]

[a] Department of Inorganic Chemistry, Physical Chemistry and Electrochemistry, Faculty of Applied Chemistry and Materials Science, University Politehnica of Bucharest, Splaiul Independentei, 313, 060042 Bucharest, Romania
[b] Department of Chemistry, University College London, 20, Gordon St., London WC1H 0AJ, United Kingdom

ARTICLE INFO

Article history:
Received 25 August 2015
Received in revised form 15 October 2015
Accepted 1 November 2015
Available online 10 November 2015

Keywords:
Nanodiamond
Solvents
Spectroscopy

ABSTRACT

In situ Attenuated Total reflectance infrared (ATR IR) spectroscopy is used to study the interaction between ethanol vapour and oxidised nanodiamond (ND) surfaces. On initial exposure an amorphous multilayer of adsorbed ethanol is observed, but over *ca.* 30 min a loss in intensity of ν(OH) and δ(OH) bands indicates a preferential binding of the ethanol –OH with the ND surface. Other spectral changes indicate ordering of the ethanol molecules on the surface and their confinement within the pores of the ND structure in specific conformations. Changes in the IR spectrum also suggest that vibrational frequencies of carbonyl groups on the ND surface are affected by the adsorption of ethanol and that surface-bound water is either displaced or involved in hydrogen-bonding with ethanol.

1. Introduction

Detonation nanodiamond (ND) is a powder composed of individual 5–10 nm diameter diamond nanoparticles. Due to the oxidative purification methods used during synthesis, the surface of the as-received ND particle is typically highly functionalised with an array of oxygen-containing moieties including carboxylic acids, anhydrides, esters, lactones, ketones and alcohols. These surface groups have been characterised with Fourier transform infra-red (FTIR) [1–3] and Raman spectroscopy [4,5], X-ray photoelectron spectroscopy (XPS) [6], and other techniques [7,8]. An advantage of the rich surface chemistry of ND is that it is amenable to functionalisation, through established organic synthetic coupling chemistry or via non-covalent attachment of suitable reagents [9]. Many of the proposed applications of ND exploit the versatility offered by the complex surface chemistry of the particles [10]. Recent proposed uses of ND include as drug delivery vehicles [11], strengthening components of polymer composites [12], sorption agents in chromatography [13] and in humidity sensors [14]. In all of these examples, an understanding of the interaction between the surface of ND particles and a solvent environment is essential to their exploitation. Depending on surface functionalisation and environment the ND particles may interact more strongly with each other than with the solvent, leading to particle agglomeration, or preferential binding of adsorbates may take place in one solvent compared to another.

To better understand the properties of ND in solution it is therefore essential to determine how solvent molecules interact with the ND surface. In this study we use attenuated total reflectance (ATR) IR spectroscopy to monitor *in situ* the interaction between ethanol molecules and highly oxidised ND powders. The use of high surface area ND powders results in greater sensitivity of this technique to the structure and bonding at the ND interface [3]. Most previous studies concerning ND-solvent interactions have focussed on water [15–20], although surface adsorption studies of ionic liquids [21], phospholipids [22], proteins [23] and mineral oils [24] have also been reported. Adsorption of water on the ND surface has been investigated with FTIR spectroscopy [15], Raman and photoluminescence spectroscopy [16], X-ray absorption and emission spectroscopy [17], permittivity measurements [18], interferometry [19] and differential scanning calorimetry [20]. A particularly strong hydrogen-bonding interaction between oxidised ND and water has been identified, leading to the formation of a surface-confined nanophase of water. This layer of surface-bound water is estimated at *ca.* 0.5 nm thickness [19] and requires prolonged heating at temperatures of up to 200 °C to be removed [15].

In this study the interaction of ethanol vapour with ND powder is investigated. Unlike water, ethanol molecules have hydrophobic, non-polar alkyl groups as well as polar, hydrophilic –OH groups and so are likely to exhibit preferential orientation in how they interact with the ND surface and with each other. It is found that initial exposure of ND to ethanol vapours results in saturation of the surface with multilayers of amorphous 'liquid' alcohol. However, a restructuring of the adsorbed layers takes place within 30–40 min, with a loss of ethanol –OH

* Corresponding author.
E-mail address: k.b.holt@ucl.ac.uk (K.B. Holt).

http://dx.doi.org/10.1016/j.diamond.2015.11.001

vibrational modes suggesting strong hydrogen bonding to the ND surface, along with evidence of ethanol molecules becoming confined within the porous structure of the ND powder.

2. Experimental

2.1. Materials and instrumentation

ND (described as 10 nm mean particle size, >97%) was purchased from Sigma-Aldrich (Dorset, England). Ethanol (>99.5%) was purchased from Merck (Darmstadt, Germany).

Mid-infrared spectra were recorded (100 scans) in ATR mode using a Bruker Tensor 27 FTIR spectrometer, fitted with a room temperature DLaTGS detector at 4 cm^{-1} resolution. The ATR accessory consisted of a diamond prism operating with one reflection. Background spectra were collected prior to each experiment (100 scans). The diamond prism was cleaned between each experiment by washing and wiping the prism, first with methanol, followed by *iso*-propanol and finally water. Whatman® 105 lens cleaning tissues 100 × 150 mm (Maidstone, England) were used for cleaning the ATR prism, which was thoroughly dried between each step with a stream of N_2 (house supply). A Carbolite MTF 1200 horizontal tube furnace was used to pre-treat and oxidise the ND sample. The temperature control unit and associated electronics were designed and built in house. TEM images were recorded using a Jeol JEM 2100 TEM with a 200 kV accelerating voltage using a LaB6 filament. Holey carbon film (50, S147A3) coated copper TEM grids were used as the nanoparticle support (Agar Scientific). Characterisation of the ND was carried out using XPS with a Thermo Scientific K-Alpha XPS system and a monochromated Al K-alpha source (E = 1486.6 eV). High resolution XPS spectra were processed and analysed using CasaXPS (version 2.3.16, Casa Software Ltd.). Spectra were fit with Gaussian–Lorentzian curves, the shape of all peaks is assumed to be 70% Gaussian and 30% Lorentzian after subtracting a Shirley background. The full width at half maximum of all deconvoluted peaks was set equal to the main C–C peak but absolute value was not constrained.

2.2. Experimental procedure

As received ND powder was treated in a furnace at 425 °C for 4 h (including temperature ramp times, which were set at 10 °C min^{-1}) in air prior to all experiments. This was to remove any sp^2 graphitic carbon from the surface and maximise the number of oxygen terminating functional groups [4]. A ND suspension was prepared by adding the oxidised ND (1.50 μg) to deionised water (1.0 ml). The suspension was shaken and sonicated at low power, but no attempt was made to break up the primary aggregates or to produce a stable colloid. The clean, dry ATR-prism was drop-coated with the ND suspension (1 μl), which was left to dry in air to form an adherent layer before being characterised. It is difficult to determine the thickness of the resulting ND layer, but drop-coating onto similar surfaces produces relatively thick multilayers of ND powder aggregates of thickness > 10 μm, as estimated from optical microscopy. As the IR evanescent wave penetrates up to 3 μm above the diamond ATR prism it therefore probes only the ND powder layer and not the region above.

A glass gas cell was placed over the sample and dry air (1 l min^{-1}) passed over the ND layer for 1 h. Dry air was prepared by passing the air from the in-house compressed air line through a filter and a desiccant. An IR spectrum was taken of the dry ND layer and this served as the background for all subsequent spectra. The air line was then switched to bubble through a solution of ethanol before entering the gas cell, thus passing ethanol vapour over the surface of the ND layer. The concentration of ethanol in the gas flow was not measured but the vapour is assumed to be close to saturated with ethanol. IR spectra were then recorded every 90 s for a period of 2 h.

3. Results

3.1. Characterisation of ND powders with ATR FTIR, TEM and XPS

A typical ATR FTIR spectrum for the drop-cast ND layers used in these experiments is shown in Fig. 1 a.

The spectrum shows a broad peak at 3380 cm^{-1} for ν(OH); a sharper band centred at 1785 cm^{-1} for ν(C=O), and a series of overlapping features between 1462–1070 cm^{-1} attributed to a mix of bending and stretching modes for various C–C, C–H and C–O containing functionalities. These observed functionalities are in agreement with those found in the literature for oxidised detonation nanodiamonds [1–3], as reviewed recently [25]. A distinct peak at 1630 cm^{-1} is also noted, attributed to the δ(OH) vibrational mode of surface-bound water. The wide scan XPS spectrum (not shown) shows the presence of only carbon, oxygen and nitrogen in the oxidised ND sample, at 89.8, 8.6 and 1.6 at.% respectively. The high resolution XPS scan of the carbon 1s region (Fig. 1 b) can be fit with several components representing C=C (284.7 eV); C–C (286.2 eV, FWHM 2 eV); C–O–C/C–OH (287.1 eV, FWHM 2.2 eV); C=O (287.5 eV, FWHM 2 eV) and O=C–OH (289.3 eV) bonding types. These values are all shifted to *ca.* 1 eV higher binding energy that might be expected from comparison with literature values [26]. This can be attributed to some charging of the insulating sample during the XPS experiment. The range of functional groups present is therefore consistent with those observed from ATR IR spectroscopy. The TEM image in Fig. 1 c shows that the individual ND particles on average around 5 nm in diameter and are highly aggregated. These aggregates cannot be broken up using the low-power sonication used in our sample preparation [25] and so it assumed that the drop-cast ND layer consists of aggregates of varying size with the primary aggregate being held together by strong attractive Coulombic attraction.

3.2. In situ ATR-IR studies of ND powder films in ethanol vapour

3.2.1. IR spectrum after 2 min exposure to ethanol vapour

Fig. 2 shows different regions of the IR spectrum of the ND layer at t = 2 min and t = 60 min after first exposure to the ethanol vapour. Note that these spectra are difference spectra; they are recorded using the spectrum of the dry ND powder layer as the background so reflect *changes* at the ND surface after ethanol exposure. After 2 min of exposure the IR spectrum reveals bands consistent with those for liquid ethanol [27] and is remarkably similar to that reported for multilayer amorphous ethanol ices formed on highly orientated pyrolytic graphite at low temperatures (80 K) [28]. The time taken to record a scan is about 90 s, hence monolayer deposition or cluster deposition at isolated sites may take place over shorter time scales than we can measure; however it appears that multilayer adsorption of ethanol on ND dominates very quickly after initial exposure.

At t = 2 min, the 3750–2750 cm^{-1} region of the IR spectrum (Fig. 2 a) shows a broad band centred at 3325 cm^{-1} that can be assigned to the ν(OH) stretch of the adsorbed ethanol. A series of overlaid, sharp bands are observed at lower wavenumbers; these can be assigned as $\nu_a(CH_3)$ and $\nu_s(CH_3)$ at 2973 cm^{-1} and 2925 cm^{-1} respectively and the unresolved band at 2885 cm^{-1} is assigned to $\nu_a(CH_2)$ and $\nu_s(CH_2)$, which have been reported previously at 2896 and 2875 cm^{-1} [27,28]. The 1550–1150 cm^{-1} region (Fig. 2 b) shows weaker bands; these are assigned to $\delta_a(CH_3)$ modes at 1479 cm^{-1} and 1450 cm^{-1}; $\delta_s(CH_3)$ at 1378 cm^{-1}; δ(OH) at 1323 cm^{-1} and $\tau(CH_2)$ at 1272 cm^{-1}. In the 1150–1000 cm^{-1} region (Fig. 2 c) strong, distinctive bands for the CH_3 rocking mode $\rho(CH_3)$ (1090 cm^{-1}) and ν(CO) stretch (1050 cm^{-1}) are observed. The band positions and assignments are summarised in Table 1, along with the position of bands observed for multilayer amorphous ethanol layers [28] and ethanol in inert gas matrices [29,30] reported in previous studies.

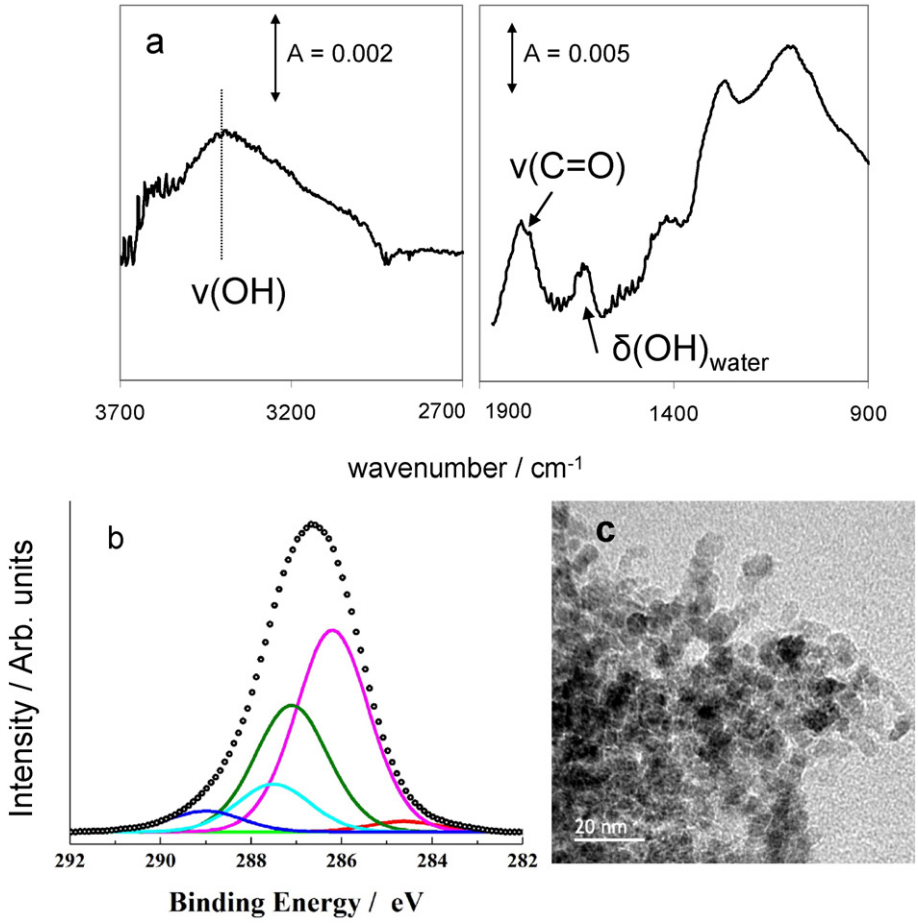

Fig. 1. (a) ATR-FTIR spectrum for a ND drop-cast dry powder film, with important features and their corresponding functionalities highlighted. (b) High resolution C 1s XPS spectrum with constituent peaks fitted: C–C (red); C–OH (pink); C–O–C (green); C=O (turquoise); O=C–OH (dark blue). (b) TEM image of the ND used in this study (1 μl of a 1.50 mg ml^{-1} solution drop-cast onto a carbon-coated copper grid).

3.2.2. Time dependence of IR response under ethanol vapour

Surprisingly, with increasing time of exposure to the ethanol vapour, the infrared bands for adsorbed ethanol decrease, rather than increase in intensity. In Fig. 3 the absorbance maximum relative to its value at t = 2 min ($\Delta A_t/\Delta A_{t\ =\ 2\ min}$) is plotted *versus* time for the ν(OH), ν(C–O) and $\rho(CH_3)$ bands. The ν(C–O) and $\rho(CH_3)$ bands show a similar relationship, whereby the absorbance decreases to *ca.* 55% of their original value over the 2 h of the experiment. Over the same time period the ν(OH) band undergoes a more drastic decrease in relative absorbance, reaching about 30% of its initial value within 30–40 min of exposure to ethanol. These observations suggest that although the ND surface is saturated immediately with multilayers of ethanol, there is no further accumulation after this initial deposition. In fact, it seems that the opposite is true; some ethanol desorbs from the surface during the course of the experiment. When the same experiment is carried out with a bare ATR prism (*i.e.* without the drop-coated layer of ND) the surface is likewise immediately saturated with multilayers of ethanol. However thereafter the intensity of the ethanol bands remains relatively constant over time, without the dramatic loss in intensity noted in the presence of ND.

Inspection of the IR spectrum for the ND layer after 60 min exposure to ethanol reveals that a change in composition of the adsorbed layer has taken place. As well as the clear loss of the ν(OH) band at 3325 cm^{-1} (Fig. 2 a) there is a less-clear concomitant loss in the weak δ(OH) band at 1323 cm^{-1} (Fig. 2 b). Additionally, there is now a small band present at 3666 cm^{-1} that does not appear in the spectrum at t = 2 min. The $\nu(CH_3)$ and $\nu(CH_2)$ regions also show changes; a clear shoulder is present at *ca.* 2995 cm^{-1}, to the high wavenumber side of the 2973 cm^{-1} peak. The peak at 2925 cm^{-1} is reduced in prominence and the broad peak at 2885 cm^{-1} at t = 2 min is now clearly resolved into 2 peaks at 2896 and 2875 cm^{-1}. In Fig. 2 b the $\delta_s(CH_3)$ band at 1380 cm^{-1} is reduced in magnitude and broadened to the higher wavenumber side by a new peak at *ca.* 1410 cm^{-1}. The $\tau(CH_2)$ peak at 1272 cm^{-1} is less defined than at t = 2 min and broadened to the low wavenumber side; a new overlapping band is now present at *ca.* 1230 cm^{-1}. In the ν(CO) and $\rho(CH_3)$ regions (Fig. 2 c) the band at 1090 cm^{-1} is weakened and broadens to the lower wavenumber side, with a shoulder emerging at *ca.* 1080 cm^{-1}. The absorbance of the 1050 cm^{-1} ν(CO) stretch is significantly decreased over time and a new small peak is observed at 1066 cm^{-1}. The positions of the peaks at t = 60 min are summarised in Table 1. Additional spectra for t = 2 min to t = 120 min are available in Supplementary information.

3.2.3. Changes to the ND surface on exposure to ethanol vapours

As the IR spectrum of the dry ND layer prior to ethanol exposure is used as the background spectrum for these experiments, changes to the surface chemistry of the ND itself can be monitored as a function of ethanol exposure. Due to the strong absorbance of ethanol over most spectral ranges, changes attributed to the ND surface rather than adsorbed ethanol are difficult to distinguish. However, in the 1880–1550 cm^{-1} region of the IR spectrum the carbonyl stretches ν(C=O) of ND are detectable and ethanol vibrational modes are not present, hence spectral changes can be attributed to changes in ND surface bonding. Fig. 4 shows the difference IR spectrum of this region at t = 2 min after ethanol exposure. The dotted horizontal line shows the position of zero absorbance; hence it is clear that a *decrease* in absorbance compared to the dry ND is noted at *ca.* 1640 cm^{-1} and 1850 cm^{-1}

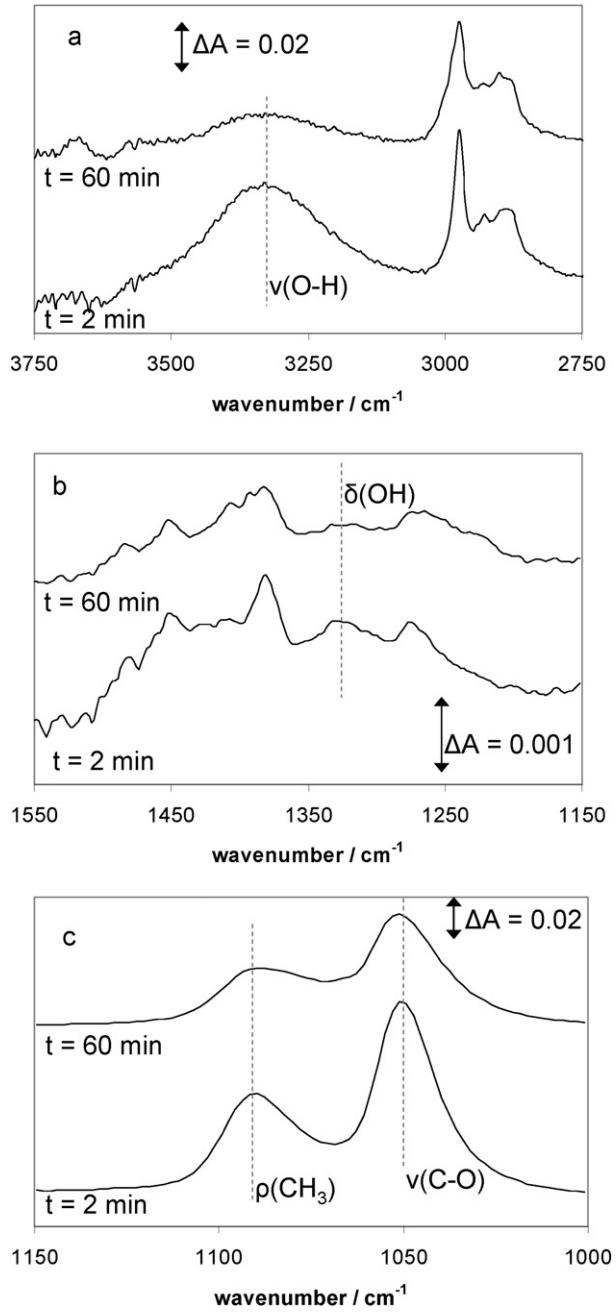

Fig. 2. ATR IR difference spectra recorded t = 2 min and t = 60 min after exposure of dry ND layer to ethanol saturated vapour. Background spectrum in each case is the dry ND layer: (a) 3750–2750 cm^{-1} region; (b) 1550–1150 cm^{-1} region; (c) 1150–1000 cm^{-1} region.

and an *increase* in absorbance is seen at *ca.* 1780 cm^{-1}. Note that the IR bands in this region are very weak, as can be seen by contrasting the ΔA scale with those in Fig. 2; nonetheless the changes can clearly be observed above the background noise and the response is reproducible, being observed in 3 separate experiments. Unlike the bands attributed to adsorbed ethanol, the spectrum in this region does not change over time, being essentially identical at t = 2 min until t > 60 min.

Bands in the region 1700–1880 cm^{-1} can be attributed to ν(C=O) stretches of the carbonyl functionalities of the ND surface. Due to the complexity of the surface it is difficult to assign the spectral changes explicitly; however in general the species most likely to exhibit vibrational spectra above 1750 cm^{-1} are esters and acid anhydrides [31]. The concomitant loss of the 1640 cm^{-1} band points to changes in surface hydrogen-bonding, as it represents the loss of the δ(OH) mode of surface-bound water [1].

Table 1
Positions of ethanol vibrational bands in cm^{-1} in this work at t = 2 min and t = 60 min and as reported for multilayer adsorption of ethanol on HOPG and ethanol within Ar matrix.

Vibrational mode	Multilayer HOPG[a]	Ar matrix[b]	t = 2 min	t = 60 min
ν(OH)		3658		3666
	3280		3325	3325
$\nu_a(CH_3)$		2996		2995
		2985		
	2973		2973	2973
$\nu_s(CH_3)$	2927	2940	2925	2925
$\nu_s(CH_2)$	2896	2901	2885	2896
	2875	2954		2875
$\delta_a(CH_3)$	1475	#	1479	1479
$\delta_a(CH_3)$	1457	1444	1450	1450
$\omega(CH_2)$	1438	1412	#	1410
$\delta_s(CH_3)$	1380	1370	1380	1380
δ(OH)	1332		1323	1323
		1239		1230
$\tau(CH_2)$	1276	1252,1240	1272	1272
$\rho(CH_3)$	1095	1092	1090	1090
		1077		1080
		1066		1066
ν(CO)	1057	1054	1049	1051

[a] From Ref. [27].
[b] From Ref. [29].

4. Discussion

At the high ethanol concentration used in this study, multilayers of adsorbed ethanol are formed on the ND powder surface immediately after first exposure. This observation is consistent with recent studies carried out with spherical, porous activated carbons [32]. At high ethanol vapour concentrations the uptake and adsorption of ethanol on oxygen-terminated activated carbons was shown to be highly dependent on pore capacity. Thus all available pore volume rapidly filled with the adsorbate, as the ethanol molecules have a strong affinity for each other and clustering is favoured. The ND powder layer used in this study is likewise of a highly porous structure, with BET measurements from similarly functionalised ND reporting majority (90%) absorption of N_2 within pores of average size 12 nm and 10% within pores of *ca.* 1 nm [33]. Therefore it is unsurprising that similar absorption behaviours should be observed for ND powders and other porous carbon materials.

Additionally it was noted for the oxidised amorphous carbons that a strong hydrogen-bonding interaction exists between ethanol molecules

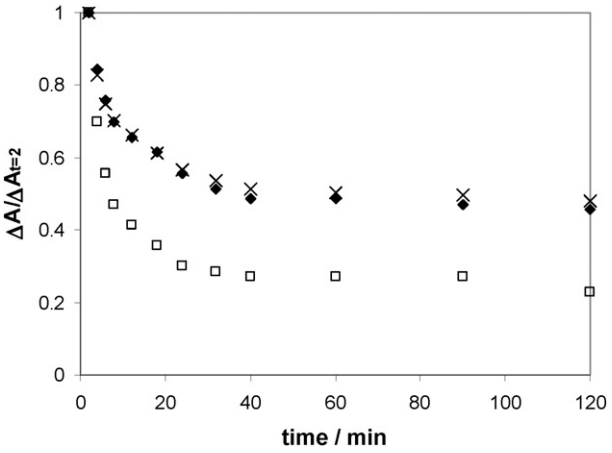

Fig. 3. Absorbance maximum relative to its value at t = 2 min ($\Delta A_t/\Delta A_{t=2\ min}$) *versus* time for the ν(OH) (open squares); ν(C–O) (crosses) and $\rho(CH_3)$ (filled circles) bands.

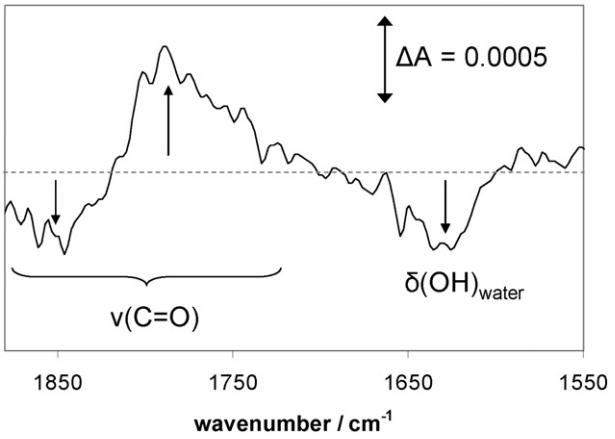

Fig. 4. ATR IR difference spectrum of 1880 cm^{-1} to 1550 cm^{-1} region recorded t = 2 min after exposure of dry ND layer to ethanol saturated vapour. Background spectrum is the dry ND layer.

and the terminating oxygen functionalities of the carbon surface. In particular, the presence of surface carboxylic acid and anhydride groups lead to enhanced adsorption of ethanol [32]. The interaction is highly favoured thermodynamically, with measured desorption energies of 50–105 kJ mol^{-1}, as measured by temperature programmed desorption [34]. This strong interaction between surface functionalities and ethanol is also evident for the ND surface, in changes we observe in the IR spectrum as the restructuring of the ethanol layer takes place over 30 min. When the ethanol molecules first adsorb on the surface they interact with both the surface and with each other; however if hydrogen-bonding to specific surface functionalities is thermodynamically favoured the molecules will reorient themselves to maximise interactions with the surface. Thus the ethanol molecules nearest the ND surface will become orientated such that the –OH groups are hydrogen-bonding with the ND surface, leaving the hydrophobic $–C_2H_5$ portions pointing away from the surface. Further from the surface ethanol molecules must interact with the surface-bound monolayer via dispersion forces, which are weak and easily overcome at ambient temperature and pressure. Therefore the more weakly bound ethanol molecules, not directly interacting with the ND surface, are likely to desorb over time and this partly explains the loss in ethanol absorbance over the first 30 min of the experiment (Fig. 3).

Decreases in IR absorbance over time will also result from the changes in orientation or ordering of the ethanol molecules. The resulting changes in symmetry cause loss in intensity of some IR modes and allow new vibrational modes to become IR active. The rapid and irreversible loss of the 3325 cm^{-1} ν(OH) and 1323 cm^{-1} δ(OH) bands indicates that an interaction between the –OH group of the ethanol and the ND is taking place, consistent with strong hydrogen-bonding of this group to the surface. As well as hydrogen-bonding, direct reaction of the ethanol molecule with the ND surface functional groups could also explain the loss of the ν(OH) and δ(OH) IR modes. On metal oxide surfaces, such as Al_2O_3 and MgO, adsorbed ethoxide species are identified by distinctive IR ν(CO) stretches at *ca.* 1125 cm^{-1} [35]. Formation of such species requires basic surface groups that can deprotonate the ethanol and a metal centre coordination site for the resulting ethoxide. In the case of the ND used in this study, we cannot detect by XPS a sufficient availability of metal centres that would support such a coordination and the ethoxide ν(CO) stretch is not observed at 1125 cm^{-1}. Therefore it seems unlikely that a surface bound ethoxide species is formed and loss of the OH vibrational modes is unlikely to be related to such a reaction.

Another explanation for the loss of the OH bands is a nucleophilic addition of the ethanol molecule to ND surface anhydrides, with resulting formation of an ester. Inspection of the ν(C=O) spectral region (Fig. 4) shows small changes indicating that vibrational frequencies of ND surface carbonyl groups are altered on exposure to ethanol. It is clear, therefore that an interaction between some surface functionalities and the adsorbate takes place. One interpretation of the observed changes could be a loss of anhydride species (1850 cm^{-1}) and gain of ester (1780 cm^{-1}). This would suggest that a small amount of the adsorbed ethanol reacts with some surface anhydride groups almost immediately on adsorption. However, as there are no further changes over time, if such a reaction takes place it is not related to the structural changes associated with loss of the ν(OH) ethanol bands, as they take place over a longer timescale. The changes to the ν(C=O) region may also be attributed to changes in the hydrogen bonding environment at the ND surface, as increase or decrease in the strength of hydrogen-bonding can lead to shifts in the ν(C=O) wavenumber and intensity changes. The other change of note in this spectral region (Fig. 4) is the loss of the δ(OH) band for surface-bound water at *ca.* 1640 cm^{-1}. Unless heated, a strongly bound nanophase of water remains associated with the ND surface and so is highly likely to present throughout these experiments [18–20]. Some bound water is likely to be associated with surface carbonyl functionalities, hence loss of the water on exposure to ethanol suggests either loss of those functionalities, displacement of water by ethanol, or an additional hydrogen-bonding interaction between the bound water molecule and the ethanol, leading to loss of the $\delta(OH)_{water}$ vibrational mode.

The restructuring of the adsorbed ethanol layer over time is indicated by the emergence of new ethanol bands over time. The positions of the new ethanol bands are very similar to those reported for studies of ethanol prepared in Ar or N_2 matrices [29,30]. In inert gas matrices the ethanol molecules are confined within the inert medium and therefore adopt different conformers: trans and gauche, depending on the orientation of the O–H bond relative to the rest of the molecule. The different molecular orientations, as well as 'wall' effects (how the molecules interact with the confining matrix) leads to distinctive splitting and shifting of IR bands, as listed in Table 1. Additionally the ν(OH) stretch of 'free' (*i.e.* non-hydrogen bonded) OH is expected for molecules in this environment. The IR spectrum of the ND-adsorbed ethanol at t = 60 min seems to be a superposition of the spectra for multilayer ethanol and matrix-confined ethanol. The confinement of ethanol molecules in pores of hydrophobic carbonaceous materials has been well-studied by different techniques [36,37] and such confinement gives rise to preferred orientations of the ethanol molecule within the pores. For the ND powder layer in this study, it could be imagined that a porous ND structure coated with ethanol molecules would give rise to a network of hydrophobic pores. The ethanol molecules adsorbed in the ND surface will orient such that their –OH bonds are close to the ND surface and the $–C_2H_5$ groups pointing away. If the entirety of the ND porous structure is covered with such a layer, this effectively leaves a network of pores with the hydrophobic $–C_2H_5$ pointing outwards, resulting in an array of hydrophobic cavities (Fig. 5). Ethanol molecules trapped within such pores would be expected to have similar IR spectra to those confined within Ar or N_2 matrices, as they are similarly confined and to show preference for different conformers. Hence the resulting IR spectrum at t = 60 min is a superposition of ethanol hydrogen-bonded to the ND surface functionalities/bound water, a further layer of amorphous multilayer ethanol and ethanol confined within pores with specific orientations.

5. Conclusions

This *in situ* study shows that ATR IR spectroscopy is an ideal technique with which to study the interaction of solvent molecules with ND surfaces. Here we have shown that ethanol shows preferential binding to the ND surface *via* the polar –OH group and that changes to the surface adsorbed layer take place over time that can be related to the ND functional groups and porous nature of the powder. Although ND is proposed for many high impact applications there is still much to understand about the interaction of these nanoparticles with their

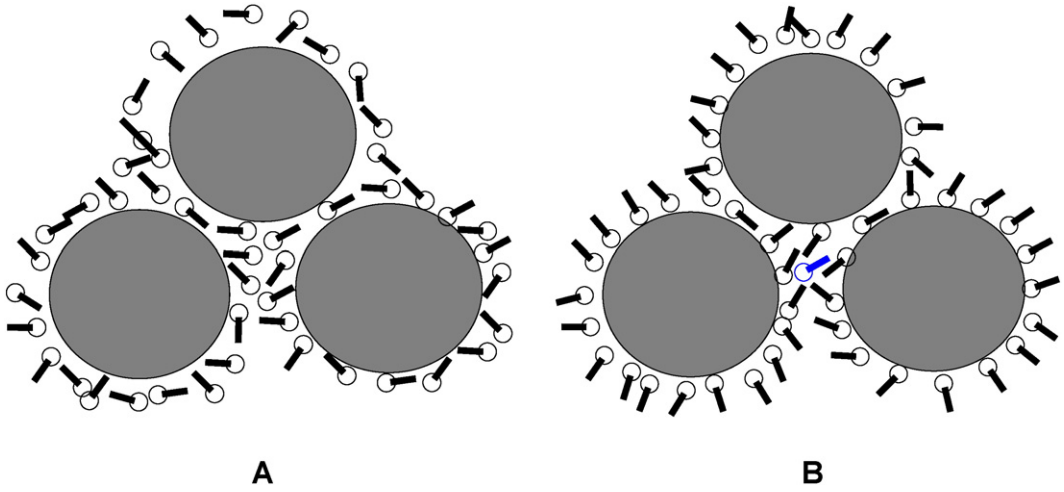

Fig. 5. Schematic (not to scale) of the arrangement of surface adsorbed ethanol molecules around ND particles. Open circles indicate hydrophilic –OH group; black sticks represent hydrophobic $-C_2H_5$ groups. A. Start of experiment, ethanol molecules arranged with random orientation around the ND surfaces (only monolayer shown for clarity, although multilayer adsorption is observed). B. After t = 60 min ethanol molecules orientate so that hydrophilic –OH can hydrogen-bond to ND surface. Hydrophobic pores are formed in which ethanol molecules can be confined (confined molecule shown in blue).

environment and particularly the solvent. We are presently undertaking studies to determine how other solvent molecules interaction with the ND surface and how the nature of the surface functional groups influences adsorption. As the surface of ND has many similarities to other forms of carbon, the conclusions from this study are applicable to oxidised nanocarbons in general, for example porous activated carbons and graphene oxide.

Supplementary data to this article can be found online at http://dx.doi.org/10.1016/j.diamond.2015.11.001.

Acknowledgements

The authors are grateful for the financial support from UEFISCDI project ID 236/2014, and the work done by Drd. Georgiana-Anca INEL has been supported by the Sectorial Operational Programme Human Resources Development 2007-2013 (InnoRESEARCH) 132395, financed from the European Social Fund and the Romanian Government under the contract number POSDRU/159/1.5/S/132395. The authors also acknowledge EPSRC grant EP/J010006/1 for partial funding of this project.

References

[1] T. Jiang, K. Xu, S. Ji, J. Chem, FTIR studies on the spectral changes of the surface functional groups of ultradispersed diamond powder synthesized by explosive detonation after treatment in hydrogen, nitrogen, methane and air at different temperatures, Soc. Faraday Trans. 86 (1990) 3401–3406.
[2] J.S. Tu, E. Perevedentseva, P.H. Chung, C.L. Cheng, Size-dependent surface CO stretching frequency investigations on nanodiamond particles, J. Chem. Phys. 125 (2006) 174713–174717.
[3] J. Scholz, A.J. McQuillan, K.B. Holt, Redox transformations at nanodiamond surfaces revealed by in situ infrared spectroscopy, Chem. Commun. 47 (2011) 12140–12142.
[4] V. Mochalin, S. Osswald, Y. Gogotsi, Contribution of functional groups to the Raman spectrum of nanodiamond powders, Chem. Mater. 21 (2009) 273–279.
[5] S. Prawer, K.W. Nugent, D.N. Jamieson, J.O. Owra, L.A. Bursill, J.L. Peng, The Raman spectrum of nanocrystalline diamond, Chem. Phys. Lett. 332 (2000) 93–97.
[6] O. Shenderova, A.M. Panich, S. Moseenkov, S.C. Hens, V. Kuznetsov, H.-M. Vieth, Hydroxylated detonation nanodiamond: FTIR, XPS, and NMR studies, J. Phys. Chem. C 115 (2001) 19005–19011.
[7] X.W. Fang, J.D. Mao, E.M. Levin, K. Schmidt-Rohr, Nonaromatic core–shell structure of nanodiamond from solid-state NMR spectroscopy, J. Am. Chem. Soc. 131 (2009) 1426–1435.
[8] M. Ozawa, M. Inaguma, M. Takahashi, F. Kataoka, A. Kruger, E. Osawa, Preparation and behavior of brownish Clear Nanodiamond Colloids, Adv. Mater. 19 (2007) 1201–1206.
[9] A. Krueger, D. Lang, Functionality is key: recent progress in the surface modification of nanodiamond, Adv. Funct. Mater. 22 (2012) 890–906.
[10] V.N. Mochalin, O. Shenderova, D. Ho, Y. Gogotsi, The properties and applications of nanodiamonds, Nat. Nanotechnol. 7 (2012) 11–23.
[11] V. Vaijayanthimala, D.K. Lee, S.V. Kim, A. Yen, N. Tsai, D. Ho, H.-C. Chang, O. Shenderova, Nanodiamond-mediated drug delivery and imaging: challenges and opportunities, Expert Opin. Drug Deliv. 12 (2015) 735–749.
[12] E. Tamburri, V. Guglielmotti, R. Matassa, S. Orlanducci, S. Gay, G. Reina, M.L. Terranova, D. Passeri, M. Rossi, Detonation nanodiamonds tailor the structural order of PEDOT chains in conductive coating layers of hybrid nanoparticles, J. Mater. Chem. C. 2 (2014) 3703–3716.
[13] A.A. Peristyy, O.N. Fedyanina, B. Paull, P.N. Nesterenko, Diamond based adsorbents and their application in chromatography, J. Chromatogr. A 1357 (2014) 68–86.
[14] Y. Yao, Y. Xue, Impedance analysis of quartz crystal microbalance humidity sensors based on nanodiamond/graphene oxide nanocomposite film, Sensors Actuators B Chem. 211 (2015) 52–58.
[15] S. Ji, T. Jiang, K. Xu, S. Li, FTIR study of the adsorption of water on ultradispersed diamond powder surface, Appl. Surf. Sci. 133 (1998) 231–238.
[16] T.A. Dolenko, S.A. Burikov, J.M. Rosenholm, O.A. Shenderova, I.I. Vlasov, Diamond–water coupling effects in Raman and photoluminescence spectra of nanodiamond colloidal suspensions, J. Phys. Chem. C 116 (2012) 24314–24319.
[17] T. Petit, M. Pflüger, D. Tolksdorf, J. Xiao, E.F. Aziz, Valence holes observed in nanodiamonds dispersed in water, Nanoscale 7 (2015) 2987–2991.
[18] S.S. Batsanov, S.M. Gavrilkin, A.S. Batsanov, K.B. Poyarkov, I.I. Kulakova, D.W. Johnson, B.G. Mendis, Giant dielectric permittivity of detonation-produced nanodiamond is caused by water, J. Mater. Chem. 22 (2012) 11166–11172.
[19] S.S. Batsanov, E.V. Lesnikov, D.A. Dan'kin, D.M. Balakhanov, Water shells of diamond nanoparticles in colloidal solutions, Appl. Phys. Lett. 104 (2014) 133105.
[20] M.V. Korobov, N.V. Avramenko, A.G. Bogachev, N.N. Rozhkova, E. Osawa, Nanophase of Water in Nano-Diamond Gel, J. Phys. Chem. C 111 (2007) 7330–7334.
[21] C.-L. Park, A.Y. Lee, M. Lee, S.-G. Lee, Gelation, functionalization, and solution behaviors of nanodiamonds with ionic liquids, Chem. Commun. (2009) 5576–5578.
[22] A. Chakraborty, N.J. Mucci, M.L. Tan, A. Steckley, T. Zhang, M.L. Forrest, P. Dhar, Phospholipid composition modulates carbon nanodiamond-induced alterations in phospholipid domain formation, Langmuir 31 (2015) 5093–5104.
[23] M. Aramesh, O. Shimoni, K. Ostrikov, S. Prawer, J. Cervenka, Surface charge effects in protein adsorption on nanodiamonds, Nanoscale 7 (2015) 5726–5736.
[24] N.A. Burns, M.A. Naclerio, S.A. Khan, A. Shojaei, S.R. Raghavan, Nanodiamond gels in nonpolar media: colloidal and rheological properties, J. Rheol. 58 (2014) 1599–1614.
[25] N.O. Mchedlov-Petrossyan, N.N. Kamneva, A.I. Marynin, A.P. Kryshtal, E. Osawa, Colloidal properties and behaviors of 3 nm primary particles of detonation nanodiamonds in aqueous media, Phys. Chem. Chem. Phys. 17 (2015) 16186.
[26] S. Ferro, M. Dal Colle, A. De Battisti, Chemical surface characterization of electrochemically and thermally oxidized boron-doped diamond film electrodes, Carbon 43 (2005) 1191–1203.
[27] E.K. Plyler, Infrared spectra of methanol, ethanol, and n-propanol, J. Res. Natl. Inst. Stan. 48 (1952) 281–286.
[28] D.J. Burke, A.J. Wolff, J.L. Edridge, W.A. Brown, The adsorption and desorption of ethanol ices from a model grain surface, J. Chem. Phys. 128 (2008) 104702–104712.
[29] A.J. Barnes, H.E. Hallam, Infra-red cryogenic studies. Part 5.—ethanol and ethanol-d argon matrices, Trans. Faraday Soc. 66 (1970) 1932–1940.
[30] G.A. Pitsevich, I.Y. Doroshenko, V.Y. Pogorelov, V. Sablinskas, V. Balevicius, Structure and vibrational spectra of gauche- and trans-conformers of ethanol: nonempirical anharmonic calculations and FTIR spectra in argon matrices, Low Temp. Phys. 39 (2013) 389–400.
[31] G. Socrates, Infrared and Raman characteristic frequencies, 3rd ed. John Wiley & Sons, Ltd., 2001
[32] A.J. Romero-Anaya, M.O. Lillo-Ródenas, A. Linares-Solano, Factors governing the adsorption of ethanol on spherical activated carbons, Carbon 83 (2015) 240–249.

[33] S.A. Denisov, G.A. Sokalina, G.P. Bogatyreva, T.Y. Grannkiva, O.K. Krasil'nikova, E.V. Plotnikova, B.V. Spitsyn, Adsorption and electrical properties of nanodiamond powders in the presence of water vapor, Prot. Met. Phys. Chem. 49 (2013) 286–291 (+).
[34] C.M. Ghimbeu, R. Gadiou, J. Dentzer, D. Schwartz, C. Vix-Guterl, Influence of surface chemistry on the adsorption of oxygenated hydrocarbons on activated carbons, Langmuir 26 (2010) 18824–18833.
[35] S. Hanspal, Z.D. Young, H. Shou, R.J. Davis, Multiproduct steady-state isotopic transient kinetic analysis of the ethanol coupling reaction over hydroxyapatite and magnesia, ACS Catal. 5 (2015) 1737–1746.
[36] T. Okhubo, T. Iiyama, K. Nishikawa, T. Suzuki, K. Kaneko, Pore-width-dependent ordering of C_2H_5OH molecules confined in graphitic slit nanospaces, J. Phys. Chem. B 103 (1999) 1859–1863.
[37] Q. Shao, L. Huang, J. Zhou, L. Lu, L. Zhang, X. Lu, S. Jiang, K.E. Gubbins, Y. Zhu, W. Shen, Molecular dynamics study on diameter effect in structure of ethanol molecules confined in single-walled carbon nanotubes, J. Phys. Chem. C 111 (2007) 15677–15685.